The Bifurcation of Outflows

DORON NOF

Department of Oceanography, The Florida State University, Tallahassee, FL 32306

(Manuscript received 30 October 1985, in final form 16 May 1986)

ABSTRACT

The behavior of outflows resulting from channels cutting through broad continents and emptying into wedgelike oceans, or channels cutting in wedgelike continents and emptying into broad oceans, is examined analytically. The model is nonlinear and inviscid, and the vertical structure is approximated by two layers; the upper layer is active and the lower is passive.

Examination of the governing equations shows that, since outflows are externally driven (by gravity and mass flux), there exists an "outflow length scale" in the open ocean. This length scale (l) is given by $[g'Hb/fU_0]^{1/2}$, where b is half the emptying channel width, g' the "reduced gravity," H the channel depth, f the Coriolis parameter, and U_0 the flow speed within the channel. Solutions are constructed using this new length scale and a power series expansion.

It is found that, due to the earth's rotation, an outflow can be deflected toward one of the coasts or bifurcate into two branches, depending on the basin geometry. When the outflow results from a channel cutting through a broad continent and emptying into a wedgelike ocean, there are two possibilities. If the wedge opening is less than 90°, the outflow deflects to the right (looking downstream); if the wedge opening is larger than 90°, the outflow deflects to the left. In contrast, when the channel is cutting through a deltalike continent and emptying into a broad ocean, the outflow bifurcates. If the angle between the two walls bounding the ocean is less than 270°, the outflow splits into a narrow band that flows to the right and a broad current that veers to the left and penetrates into the ocean interior as an isolated ocean. A mirrored picture is established when the angle between the walls is larger than 270°.

Possible application of this theory to the two outflow modes observed near the Tsugaru Strait is mentioned.

1. Introduction

a. General description

The way that mediterranean seas and rivers empty into the ocean is an important and difficult problem. Its importance stems from the fact that it affects the distribution of salinity and nutrients up to very large distances [$\sim$O(1000 km)] away from the source. The difficulty in modeling and analyzing its behavior is a consequence of the inherent nonlinearity that results from the relative small length scale (imposed by the feeding channel) and the relatively high speeds.

Outflows spread in a variety of oceanic basins; many correspond to wedgelike oceans or continents that resemble a delta. Consider the following situation as an idealized formulation of the problem. A uniform channel whose width is $2b$ is connected to an oceanic basin bounded by two walls (Fig. 1). The angle between the basin walls and the x-axis (α) can take values larger than 90° so that the continent (through which the channel cuts) can have the shape of a delta (Δ). In the ocean, the model has two layers, a shallow (active) upper layer and a deep (passive) lower layer. It is inviscid and nondiffusive, and the motions are driven solely by the flow in the channel. Namely, the effects of wind and coastal currents are not taken into account so the basin would have been stagnant had the channel not been feeding fluid into it.

b. Background

Although the above problem has never been considered directly, there have been a number of related investigations. Takano (1954, 1955) was the first to investigate the spreading of a river in an oceanic basin. His basin occupied half of the plane and the motions were frictionally dominated. Consequently, the river plume deflects to the right in the Northern Hemisphere. Paul and Lick (1974) studied numerically the river discharge into a lake with a preexisting circulation, and Whitehead et al. (1974) examined the "hydraulic control" exerted by a strait. Beardsley and Hart (1978) have looked at the way that estuarine flow interacts with the continental shelf; Kawasaki and Sugimoto (1984) have examined, with the aid of a laboratory model, the behavior of buoyancy-driven outflows in rectangular basins.

Other investigations related to the problem posed above are those of Nof (1978a,b), who considered the effect of a sudden widening in a channel, and the transient analyses of Whitehead and Miller (1979), Stern (1980), Stern et al. (1982), and Griffith and Hopfinger (1983), all of whom considered river outflows bounded

© 1987 American Meteorological Society

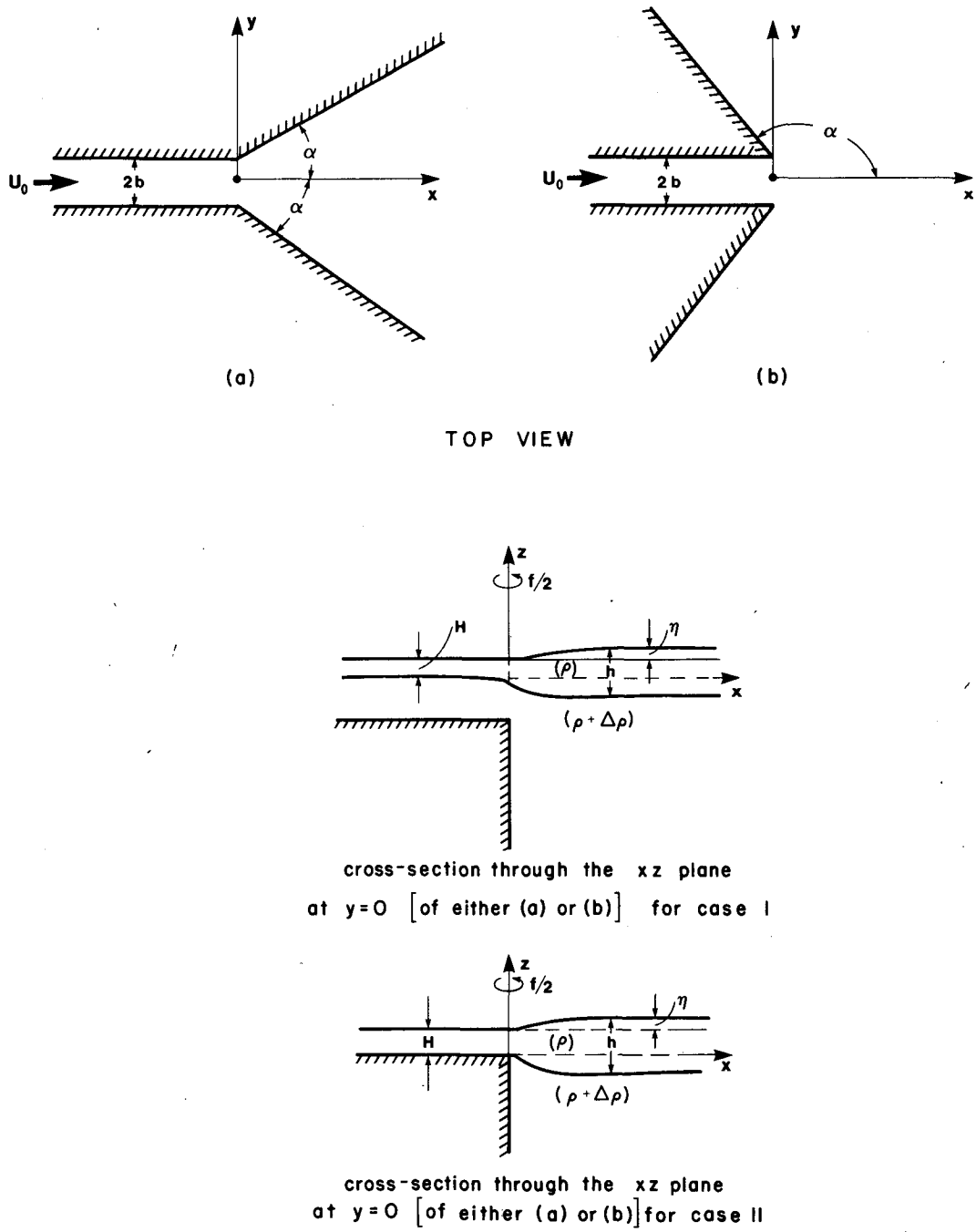

FIG. 1. Schematic diagram of the model under study. The wedge [top view (a)] and delta [top view (b)] correspond to the various basins into which outflows debouch. The free surface displacement η is measured upward from the undisturbed depth at the origin [i.e., $\eta(0, 0) = 0$]. H is the undisturbed depth at $x = 0$, $2b$ is the channel width.

by a front (i.e., a surfacing interface). The latter group of investigations differs from the case considered in this study because, in an infinitely wide ocean, the presence of a front tends to confine all motions to the vicinity of the right wall. Another closely related work is that of Nof (1981), who considered the dynamics of *equatorial* outflows and the way that rivers empty into (equatorial) wedgelike basins. The present study is essentially an extension of Nof (1981) to midlatitude outflows and to basins that are far broader than wedgelike seas. The techniques used in this paper are similar to those discussed by Nof (1981), and there is some

(limited) overlapping between the two articles because an attempt has been made to make the present paper self-contained.

c. Methods

The particular approach that will be used to solve for the flow in the basin is to simplify the structure of the nonlinear governing equations (the potential vorticity and the Bernoulli integral) by using a perturbation scheme in $\epsilon = 2b/l$, the ratio of the channel width ($2b$) to the length scale in the open ocean (l). We shall show that the outflow length scale (l) is not the familiar Rossby deformation radius but rather a function of the transport in the channel. Expansion of the Bernoulli integral in power series shows that up to $O(\epsilon)$, the relative vorticity equals the vorticity generated by the deepening of the upper layer in the basin. The reduced potential vorticity equation and the simplified Bernoulli integral are then combined to a second-order partial differential equation, which is solved by elementary methods and second-order polynomials.

This paper is organized as follows. The formulation of the problem is discussed in section 2. Section 3 includes a thorough discussion of the new length scale and the perturbation scheme. Section 4 contains the zero-order solution and section 5 discusses its implications. Section 6 summarizes this work.

2. Formulation

As an idealized representation of the problem, consider again the model shown in Fig. 1. As mentioned earlier, the upper layer is shallow (and active) and the lower layer is deep (and passive). Two slightly different cases are considered—the first has a two-layer structure in both the channel and the ocean (case I), whereas the second has *one layer* in the channel and two layers in the ocean (case II). Note that the fact that the lower layer is motionless does not imply that the lower-layer *transport* is small compared to the upper-layer mass flux. All it means is that the lower-layer *velocities* are small compared to the speeds in the upper layer.

The flow in the upper layer is taken to be steady, inviscid and nondiffusive, and the pressure is assumed to be hydrostatic. The x- and y-axes are directed along and across the channel's mouth, and the system rotates uniformly about the vertical axis (z). Because of the hydrostatic approximation, the horizontal velocity components (u, v) are taken to be independent of depth. For such conditions the potential vorticity equation and the Bernoulli integral are (e.g., see Gill, 1982)

$$\nabla_H \cdot (\nabla_H \psi/h) + f = hK(\psi) \tag{2.1}$$

$$\frac{1}{2}(\nabla_H \psi/h)^2 + g'h = G(\psi) \tag{2.2}$$

where $K(\psi) = dG(\psi)/d\psi$, ∇_H is the horizontal del-operator, f the Coriolis parameter, h the total upper-layer depth, g' the "reduced gravity" (equal to $g\Delta\rho/\rho$ with g the gravitational acceleration, $\Delta\rho$ the density difference between the layers and ρ the upper-layer density), and ψ a transport function defined by

$$\frac{\partial\psi}{\partial x} = vh, \quad \frac{\partial\psi}{\partial y} = -uh. \tag{2.3}$$

The transport function ψ is taken to be zero along the left feeding channel wall [i.e., $\psi(x, b) = 0$; $x \leq 0$ where b is half the feeding channel width]. The functions $K(\psi)$ and $G(\psi)$ are to be determined from the upstream conditions, which must be specified. In contrast to the cases considered by Nof (1978a,b) and Takano (1954, 1955), where it was necessary to specify the upstream conditions at the mouth, it is sufficient here to specify the upstream condition away from the outlet to the basin (i.e., as $x \to -\infty$). For both case I and case II we take the upstream flow to be uniform:

$$u_u = U_0, \quad -b \leq y \leq b, \quad x \to -\infty \tag{2.4}$$

where the subscript "u" indicates that the variable in question is associated with the upstream conditions.

Since the flow in the channel is unidirectional ($v = 0$), the y-component of the momentum equation ($u\partial u/\partial x + v\partial v/\partial y + fu = -(1/\rho)\partial p/\partial y$ where p is the hydrostatic pressure) implies that the flow is in geostrophic balance in the cross-channel direction. This means that for case I:

$$h_u = H - fU_0 y/g' \tag{2.5a}$$

$$\psi_u = \frac{g'}{2f}[h^2 - (H - fU_0 b/g')^2] \tag{2.5b}$$

where H is the undisturbed upper-layer depth in the channel.

Application of these upstream conditions (2.4)–(2.5) to (2.1) gives for case I,

$$K(\psi) = f/h(\psi) \tag{2.6}$$

which shows that

$$K(\psi) = f\Big/\left[\frac{2f\psi}{g'} + \left(H - \frac{fU_0 b}{g'}\right)^2\right]^{1/2}. \tag{2.7}$$

Similarly, application of (2.4)–(2.5) to (2.2) shows that

$$G(\psi) = \frac{1}{2}U_0^2 + g'\left[\frac{2f\psi}{g'} + \left(H - \frac{fU_0 b}{g'}\right)^2\right]^{1/2} \tag{2.8}$$

which satisfies the condition $dG(\psi)/d\psi = K(\psi)$ as required.

In view of (2.7) and (2.8), the general structure of the governing equations for case I is

$$\nabla_H \cdot \left(\frac{\nabla_H \psi}{h}\right) + f = hf\Big/\left[\frac{2f\psi}{g'} + \left(H - \frac{fU_0 b}{g'}\right)^2\right]^{1/2} \tag{2.9a}$$

$$\frac{1}{2}\left(\frac{\nabla_H \psi}{h}\right)^2 + g'h = \frac{1}{2}U_0^2 + g'\left[\frac{2f\psi}{g'} + \left(H - \frac{fU_0 b}{g'}\right)^2\right]^{1/2}. \tag{2.9b}$$

Note that these equations govern the flow in both the channel and the basin. In a similar fashion, the governing equations for case II are found to be

$$\nabla_H \cdot \left(\frac{\nabla_H \psi}{h}\right) = f(h-H)/H \tag{2.10a}$$

$$\frac{1}{2}\left(\frac{\nabla_H \psi}{h}\right)^2 + g\eta = \frac{1}{2}U_0^2 + f\psi/H - fU_0 b \tag{2.10b}$$

where H is now the channel depth and η is the free surface displacement. For simplicity, it has been assumed here that upstream at $x \to \infty$ the channel bottom is not flat but rather has a transversal slope identical to $d\eta_u/dy$. Under such conditions $h_u = H$. It will become clear later that this assumption is made merely for convenience and is not essential. It can be easily avoided by invoking the rigid-lid approximation $h_u = H + \eta \approx H$. Note that for the oceanic basin, $g\eta$ can be replaced by $g'h$.

The boundary conditions for case I are

$$\psi = 0 \quad \begin{cases} y = b, & -\infty < x \leqslant 0 \\ y = b + x\tan\alpha, & 0 \leqslant x < \infty \end{cases} \tag{2.11a}$$

$$\psi = HU_0(b-y) + fU_0^2(y^2 - b^2)/g', \quad -b \leqslant y \leqslant b, \quad x \to -\infty \tag{2.11b}$$

$$\psi = 2HU_0 b \quad \begin{cases} y = -b, & -\infty < x \leqslant 0 \\ y = -b - x\tan\alpha, & 0 \leqslant x < \infty. \end{cases} \tag{2.11c}$$

For case II the boundary conditions are identical to (2.11), except that the second term on the left-hand side of (2.11b) [i.e., $fU_0^2(y^2 - b^2)/g'$] should be omitted. In addition to the above boundary conditions, we require for both cases that all streamlines originate at the upstream section of the channel and that there are no other streamlines in the basin. This condition can be written as

$$0 \leqslant \psi(-\infty, y) \leqslant 2U_0 Hb \quad \text{for all } \psi \quad \text{and} \quad -b \leqslant y \leqslant b \tag{2.12}$$

which states that *all* ψ must possess a value between zero and $2U_0Hb$ for $x \to -\infty$ and $-b \leqslant y \leqslant b$ so that all streamlines originate in the upstream section of the channel. This condition is, in principle, equivalent to the so-called radiation condition, which allows the fluid to flow out of the basin but does not allow it to flow in. It is consistent with our formulation which addresses outflows that are driven solely by the flow originating in the channel.

It will become clear later that the outflow solution which we will shortly derive cannot fill the whole oceanic basin. Consequently, there will be regions into which the outflow does not penetrate. Namely, there are areas separated from the mean flow by a free dividing streamline. Such regions must be at rest because, in the absence of friction and time-dependent motions, there is no mechanism by which momentum can be transferred to them (e.g., see Nof 1981; Ingersoll, 1969).

3. Scaling and perturbation analysis

We shall first determine the length and velocity scale for the flow in the basin; the following analysis is relevant to both case I and case II. Since the flow in the basin is a discharge-driven flow, the velocity scale is

$$\psi_0/lH \tag{3.1}$$

where ψ_0 is the channel mass flux ($2U_0Hb$) and l is the, as yet, unknown length scale. Because of the conservation of potential vorticity, this velocity scale must also be equal to

$$u, v \sim \mathrm{O}\left(f\frac{\Delta H}{H}l\right) \tag{3.2}$$

where ΔH is the change in depth that a parcel experiences as the flow spreads in the basin. We shall now show that ΔH can be estimated with the aid of the Bernoulli integral. From (2.10) one can see that the *maximum* depth change *along a streamline* is $U_0^2/2g'$ because this is the depth change that corresponds to zero speed in the field. In other words, as the flow emerges from the channel mouth it spreads and slows down and this reduction in speed gives rise to a depth increase of $U_0^2/2g'$.

Combination of the above relationships with (3.1) and (3.2) gives

$$l = 2(g'Hb/fU_0)^{1/2}$$

or

$$l = 2R_d/(\mathrm{Ro})^{1/2} = 2b(\mathrm{Ro}/\mathrm{Fr})^{1/2} \tag{3.3}$$

where R_d is the deformation radius, $(g'H)^{1/2}/f$; Ro the channel Rossby number, U_0/bf; and Fr the Froude number, $U_0^2/g'H$. For many flows, Ro $\gg$ 1 and Fr $\ll$ 1 so that l is smaller than the deformation radius. For example, if $2b \sim 1$ km, $U_0 \sim 1.5$ m s^{-1}, $g' \sim 5 \times 10^{-2}$ m s^{-2}, $f \sim 10^{-4}$ s^{-1}, and $H \sim 200$ m, we have Ro = 30 and Fr = 0.23. The corresponding deformation radius is about 32 km, whereas the appropriate length scale l is only 12 km.

Before proceeding, it should be pointed out that if the geostrophic value is used for ΔH in (3.2) (i.e., ΔH is taken to be equal to f_0U_0b/g'), then l takes a value *identical* to the deformation radius, as should be the case. The main difference between our case and the scale of a geostrophic or quasi-geostrophic flow is that in the former the depth variations along streamlines are much larger than the geostrophic depth changes [i.e., $U_0^2/2g' \gg fU_0b/g' = fU_bl/g'$, where U_b is the velocity scale in the basin $U_0(b/l)$].

The ratio between the feeding channel width ($2b$) and the length scale in the open ocean (l) is usually small, suggesting that a perturbation expansion in $2b/l$ can be used. Such a perturbation will not only simplify the governing equations but will also simplify

the geometry of the problem. Specifically, such a perturbation will reduce the geometry to that of a point source in a wedgelike ocean. Namely, instead of considering the full problem consisting of a channel feeding into a basin, it will be sufficient to consider a point source in a wedge. To perform the perturbation expansion, the following nondimensional scaled variables are defined:

$$\left.\begin{array}{l} \hat{x}=x/l;\quad \hat{y}=y/l;\quad \hat{\psi}=\psi/2U_0Hb \\ \hat{h}=h/H;\quad \hat{u}=u/U_0(b/l);\quad \hat{v}=v/U_0(b/l) \\ \nabla=l\nabla_H;\quad \epsilon=2b/l;\quad \delta=\mathrm{Fr}/\epsilon \end{array}\right\}. \tag{3.4a}$$

We shall focus our attention on situations where

$$\left.\begin{array}{l} (\hat{x},\hat{y})\sim O(1);\ (\hat{u},\hat{v})\sim O(1);\ \hat{h}\sim O(1) \\ \hat{\psi}\sim O(1);\ \epsilon\ll 1;\ \mathrm{Fr}\sim O(\epsilon);\ \delta\sim O(1) \\ \mathrm{Ro}\sim O(1/\epsilon) \end{array}\right\}. \tag{3.4b}$$

In terms of the nondimensional variables defined by (3.4a), the governing equations for case I [i.e., Eqs. (2.9a) and (2.9b)] become

$$\frac{\epsilon\delta}{2}\nabla\cdot\left(\frac{\nabla\hat{\psi}}{\hat{h}}\right)+1=\hat{h}[(1-\epsilon^2)^2+4\epsilon^2\hat{\psi}]^{-1/2} \tag{3.5}$$

$$\frac{\epsilon\delta}{2}\left(\frac{\nabla\hat{\psi}}{\hat{h}}\right)^2+\hat{h}=\frac{\epsilon\delta}{2}+[(1-\epsilon^2)^2+4\epsilon^2\hat{\psi}]^{1/2}. \tag{3.6}$$

The nondimensional equations governing the oceanic basin associated with case II are

$$\frac{\epsilon\delta}{2}\nabla\cdot\left(\frac{\nabla\hat{\psi}}{\hat{h}}\right)=\hat{h}-1 \tag{3.7}$$

$$\frac{\epsilon\delta}{2}\left(\frac{\nabla\hat{\psi}}{\hat{h}}\right)^2+\hat{h}=\frac{\epsilon\delta}{2}+1+\epsilon^2(2\hat{\psi}-1). \tag{3.8}$$

To derive (3.8) we have replaced $g\eta$ by $g'h$ [in (2.10b)] so that it is appropriate for the basin alone. Somewhat different scaling must be used for the equations governing the motions in the channel because the lower layer is absent. It will become clear later, however, that the governing equations for the channel are not needed for the zero-order flow, and, therefore, they are not presented.

The nondimensional boundary conditions and the "radiation condition" for case I are found from (2.11) and (2.12) to be

$$\hat{\psi}=0\quad\begin{cases}\hat{y}=\epsilon, & -\infty<x\leqslant 0\\ \hat{y}=\epsilon+\hat{x}\tan\alpha, & 0\leqslant\hat{x}<\infty\end{cases} \tag{3.9a}$$

$$\hat{\psi}=\frac{1}{2}(1-\hat{y}/\epsilon)+\left[\frac{\hat{y}^2}{2}-\frac{\epsilon^2}{2}\right],\quad -\epsilon\leqslant\hat{y}\leqslant\epsilon,\ \hat{x}\to-\infty \tag{3.9b}$$

$$\hat{\psi}=1\quad\begin{cases}\hat{y}=\epsilon-\hat{x}\tan\alpha, & 0\leqslant\hat{x}<\infty\\ \hat{y}=-\epsilon, & -\infty<x\leqslant 0\end{cases} \tag{3.9c}$$

$$0\leqslant\hat{\psi}(-\infty,y)\leqslant 1\quad \text{for } all\ \hat{\psi}. \tag{3.9d}$$

As before, the boundary conditions for case II are identical to those of case I except that the term in square brackets in (3.9b) should be omitted. In addition, note that, as previously, (3.9d) indicates that all $\hat{\psi}$ intersects the line $-\epsilon\leqslant y\leqslant\epsilon$; $x\to-\infty$, ensuring that all streamlines originate upstream in the channel and there is no flow into the channel.

It is further assumed that for both case I and case II, $\hat{\psi}$ and $\hat{h}$ can be expanded in power series.

$$\left.\begin{array}{l} \hat{\psi}(\hat{x},\hat{y},\alpha,\delta,\epsilon)=\psi^{(0)}(\hat{x},\hat{y},\delta,\alpha)+\epsilon\psi^{(1)}(\hat{x},\hat{y},\delta,\alpha)+\cdots \\ \hat{h}(\hat{x},\hat{y},\alpha,\delta,\epsilon)=h^{(0)}(\hat{x},\hat{y},\delta,\alpha)+\epsilon h^{(1)}(\hat{x},\hat{y},\delta,\alpha)+\cdots \end{array}\right\}. \tag{3.10}$$

By substituting (3.10) into the Bernoulli integral (3.6), collecting terms up to $O(\epsilon^2)$, and then substituting into (3.5), one finds the following zero- and first-order equations for case I:

$$h^{(0)}=1;\quad \nabla^2\psi^{(0)}=1 \tag{3.11}$$

$$h^{(1)}=\delta/2;\quad \nabla^2\psi^{(1)}=\delta/2 \tag{3.12}$$

$$h^{(2)}=2\psi^{(0)}-1. \tag{3.13}$$

Similarly, one finds for case II:

$$h^{(0)}=1;\quad \nabla^2\psi^{(0)}=1 \tag{3.14}$$

$$h^{(1)}=\delta/2;\quad \frac{\delta}{2}\nabla^2\psi^{(1)}-\frac{\delta^2}{4}=(2\psi^{(0)}-1) \tag{3.15}$$

$$h^{(2)}=2\psi^{(0)}-1. \tag{3.16}$$

We see that, because the channel is approximated by a point source, the zero-order equations of case I (3.11) and case II (3.14) are *identical,* despite the fact that the upstream conditions are quite different. Note, however, that this is not the case for the first-order problem, where the governing equations of the two cases [(3.12) and (3.15)] do not even have the same structure. It is a simple matter to show, with the aid of (3.10) and (3.9), that the boundary conditions have similar properties. That is to say, the zero-order boundary conditions for the two cases are identical, whereas the first-order conditions are different. We shall see that the dynamics that are of present interest can be understood from the zero-order problem alone. In view of this, our attention will be focused solely on the zero-order flow and we shall keep in mind that our solution is relevant for both case I and case II.

The boundary conditions for the zero-order problem are

$$\psi^{(0)}=0;\quad \hat{y}=\hat{x}\tan\alpha,\quad 0\leqslant\hat{x}<\infty \tag{3.17a}$$

$$\psi^{(0)}=1;\quad \hat{y}=-\hat{x}\tan\alpha,\quad 0\leqslant\hat{x}<\infty \tag{3.17b}$$

$$0\leqslant\lim_{\hat{y}\to 0}\psi^{(0)}(0,\hat{y})\leqslant 1\quad \text{for all } \hat{\psi}. \tag{3.17c}$$

Note that (3.17) does not include any condition equivalent to (3.9b) because the channel width has degen-

erated to a point. In a similar fashion to (3.9d), (3.17c) ensures that all streamlines originate from the channel. Equations (3.11), (3.14) and (3.17) show that, as in Nof (1981), the perturbation scheme removed the nonlinearity from the problem and reduced the number of unknowns from two ($\hat{\psi}$ and $\hat{h}$) to one ($\psi^{(0)}$).

4. Zero-order solution

The solution of the zero-order equation (3.11) consists of a homogeneous part, $\psi_H^{(0)}$, which satisfies the Laplace equation, and a particular solution, $\psi_p^{(0)}$, whose Laplacian gives the right-hand side of (3.11). The boundary conditions for the homogeneous solution are identical to (3.17). The particular solution should vanish on both coasts and together with $\psi_H^{(0)}$ should satisfy (3.17c) everywhere if the solution is to be valid in the whole field.

The homogeneous solution $\psi_H^{(0)}$ satisfying $\nabla^2\psi_H^{(0)}$ and (3.17a–c) is found by elementary methods to be

$$\psi_H^{(0)} = \frac{1}{2}[1 - \tan^{-1}(\hat{y}/\hat{x})/\alpha] \tag{4.1}$$

which describes straight streamlines corresponding to a purely radial flow. It is important to note that this homogeneous solution corresponds to the total solution on a nonrotating plane ($f = 0$). This cannot be easily verified from (3.11) because the scaling that we have used involves ($1/f$). It can, however, be verified from the basic equations (2.9) and (2.10) by setting $f = 0$ and neglecting terms that involve the square of the velocity in the field.

The particular solution is found by noting that the Laplacian of any second-order polynomial gives a constant. It is easy to see that

$$\hat{\psi}_p^{(0)} = \frac{(\hat{y})^2 - (\hat{x})^2 \tan^2\alpha}{2(1 - \tan^2\alpha)} \tag{4.2}$$

is the only second-order polynomial that vanishes on the two coastlines ($\hat{y} = \pm\tan\alpha$). The complete solution to zero-order is, then,

$$\boxed{\psi^{(0)} = \frac{1}{2}[1 - \tan^{-1}(\hat{y}/\hat{x})/\alpha] + \frac{(\hat{y})^2 - (\hat{x})^2 \tan^2\alpha}{2(1 - \tan^2\alpha)}.} \tag{4.3}$$

This solution satisfies the governing equation (3.11) and the boundary conditions along the walls [(3.17a) and (3.17b)] for all $\hat{x}$, but, as we shall see, it satisfies the radiation condition (3.17c) only up to a certain distance from the channel mouth. Beyond this distance (4.3) is not valid, and, to satisfy the radiation condition and (3.17a–b), it is necessary to allow for separation and blocking to occur. We shall show that this results from the fact that the uniform vorticity imposes a limit on the possible growth of the outflow width. In other words, the outflow width is limited to our new length scale l. This forces a separation from the walls or a formation of stagnant regions in areas where the basin width is considerably larger than l.

The solution (4.3) possesses two singularities—one at $\alpha = \pi/4$ and the other at $\alpha = 3\pi/4$. It will be shown later that these singularities are a direct result of our perturbation analysis, which breaks down when $\alpha \to \pi/4, 3\pi/4$. To analyze the solution (4.3) and to investigate the nature of these singularities, we shall consider in section 5 outflows spreading in various basins.

5. Analysis and discussion

As pointed out earlier with regard to (4.1), the first term in (4.3) (i.e., the homogeneous solution) corresponds to the solution in the absence of rotation ($f = 0$) and the second is the contribution of the earth's rotation. The sign of the latter term depends on whether $\alpha < \pi/4$ or $\alpha > \pi/4$ and whether $\alpha < 3\pi/4$ or $\alpha > 3\pi/4$. In the first and third cases the term is positive whereas in the second and fourth cases it is negative. This shows that the direction at which rotation influences the flow crucially depends on the angle between the coastlines. For clarity, we classify four different kinds of basins,

narrow wedges: $0 \leqslant \alpha \leqslant \pi/4$

broad wedges: $\pi/4 \leqslant \alpha \leqslant \pi/2$

super broad basins: $\pi/2 \leqslant \alpha \leqslant 3\pi/4$

ultra broad basins: $3\pi/4 \leqslant \alpha \leqslant \pi$.

The behavior of the outflows spreading in these various basins is discussed below.

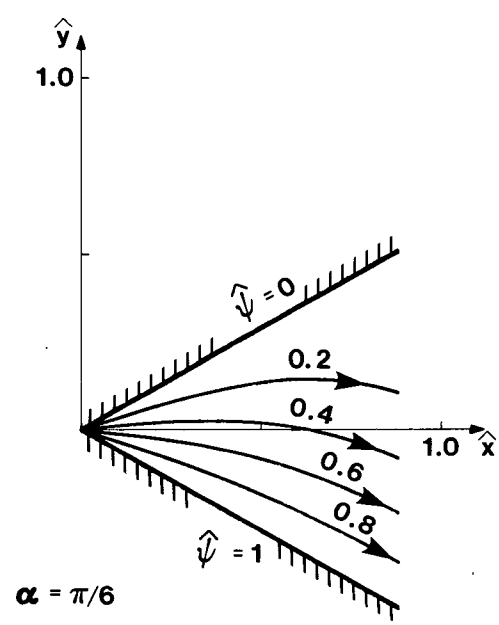

FIG. 2a. The streamfunction of an outflow spreading in a narrow basin ($\alpha < \pi/4$). The flow migrates from the center toward the right wall (looking downstream) because the constant cyclonic vorticity is offset mainly by horizontal shear (see text). Farther downstream the tendency of the flow to deflect toward the right wall becomes so great that the fluid cannot cling to the left wall (Fig. 5).

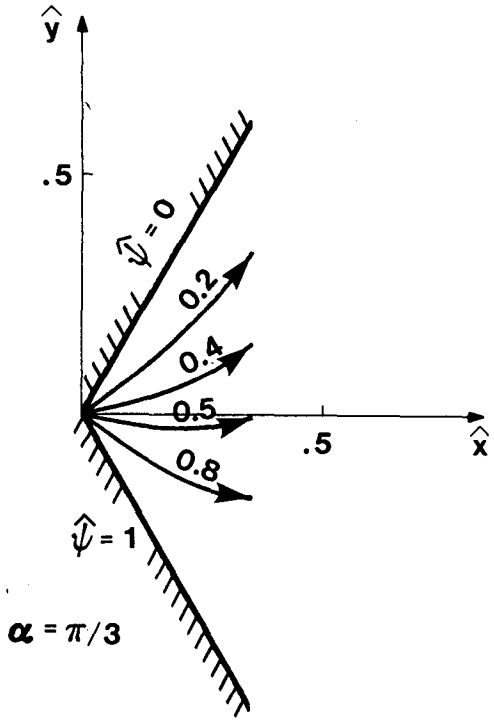

FIG. 2b. The streamfunction of an outflow spreading in a broad basin ($\pi/4 \leqslant \alpha \leqslant \pi/2$). In contrast to a narrow outflow (Fig. 2a), the flow migrates toward the left wall because the constant cyclonic vorticity is offset mainly by curvature vorticity (see text). Note that, as in Fig. 2a, the deflection tendency increases downstream. Farther downstream the deflection becomes so large that the flow separates from the right wall (Fig. 5).

a. *Narrow and broad wedges*

We shall first discuss the regions in the vicinity of the mouth where the solution (4.3) satisfies both the conditions at the walls and the radiation condition. In these regions there is no separation or blocking and (4.3) is a valid solution to the problem. For narrow wedges ($0 \leqslant \alpha \leqslant \pi/4$) the second term in (4.3) is positive and the outflow deflects to the right (Fig. 2a), whereas for broad wedges ($\pi/4 \leqslant \alpha \leqslant \pi/2$) the second term is negative and the outflow deflects to the left (Fig. 2b). This peculiar behavior results from the fact that in a narrow wedge ($0 \leqslant \alpha \leqslant \pi/4$) the vorticity generated by the spreading is compensated mainly by shear ($\partial u^{(0)}/\partial \hat{y}$), whereas in a broad wedge ($\pi/4 \leqslant \alpha < \pi/2$) the vorticity is compensated mainly by curvature vorticity ($\partial v^{(0)}/\partial \hat{x}$) (see Fig. 3). As shown in Fig. 4a, cyclonic shear tends to deflect the outflows toward the right, whereas cyclonic curvature vorticity tends to shift the current toward the left (Fig. 4b). Note that the flow pattern shown in Fig. 2a is consistent with the laboratory experiments of Stommel et al. (1958); unfor-

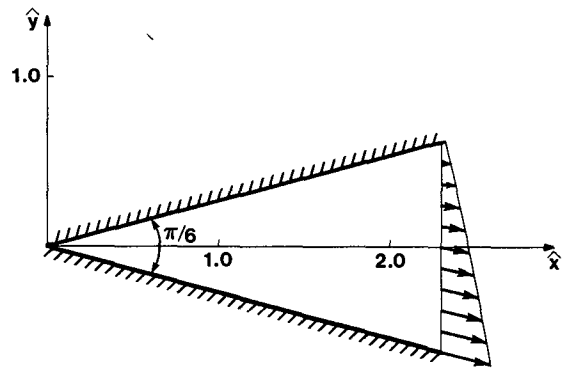

FIG. 4a. The velocity vectors in a narrow basin. Note that shear dominates, and, therefore, the flow deflects to the right.

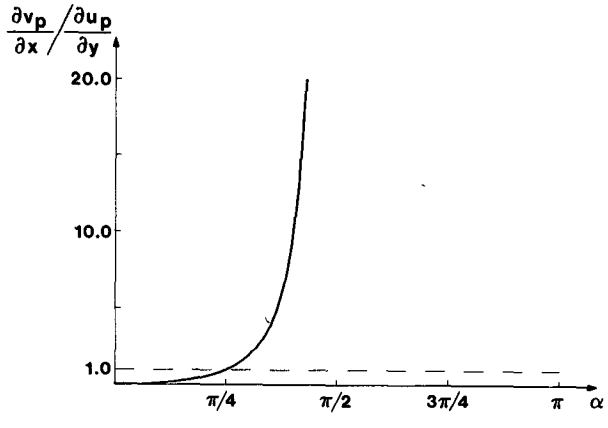

FIG. 3. The ratio between the rotational induced curvature vorticity $\partial v_p/\partial x$ to the rotational induced shear $\partial u_p/\partial y$ as a function of α. The velocities v_p and u_p are defined such that $v = u_H + v_p$ and $u = u_H + u_p$ where u_H and v_H are velocities associated with the homogeneous flow ($f = 0$). Note that shear dominates narrow basins ($\alpha < \pi/4$) whereas curvature vorticity dominates broad basins ($\pi/4 \leqslant \alpha \leqslant \pi/2$).

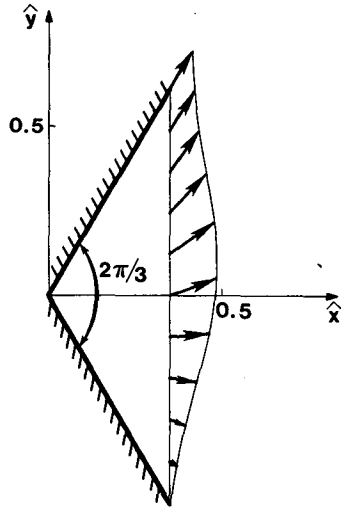

FIG. 4b. The velocity vectors in a broad basin. Note that, in contrast to Fig. 4a, curvature vorticity dominates so that the velocity vector rotates counterclockwise. Consequently, the flow deflects toward the left.

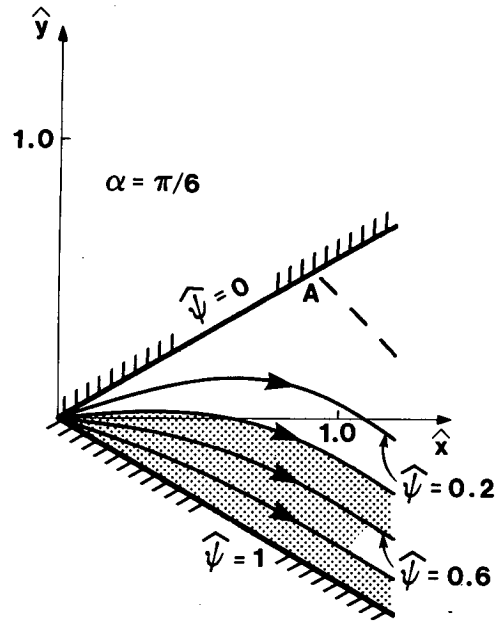

FIG. 5a. The streamlines of an outflow spreading in a narrow basin. The outflow separates from the left wall at (A). To illustrate the separation process and the formation of blocked regions, the solution is extrapolated for a short distance beyond the separation point (dashed line). The shaded area denotes the core of the outflow.

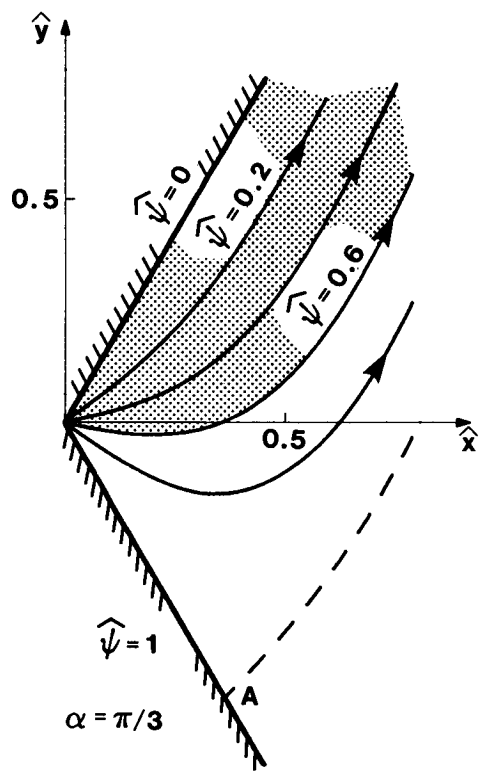

FIG. 5b. The streamlines of an outflow spreading in a broad basin. The outflow separates from the right wall at (A). As before, the separation is illustrated by extrapolating the solution for a short distance beyond the separation point (dashed line). The shaded area denotes the core of the outflow.

tunately, there have not been any experiments corresponding to broad wedges (Fig. 2b).

We shall now investigate the possibility of separation and "blocking" (the term "blocking" is used with reference to regions into which the outflow cannot penetrate). To do so we shall further examine the velocity field to see whether the solution (4.3) allows for negative velocities downstream which do not correspond to parcels that originated upstream and are, therefore, incompatible with the radiation condition (3.17c).

The horizontal velocity component in the x-direction along the left wall ($\hat{y} = \hat{x}\tan\alpha$) is found from (4.3) to be

$$\hat{u} = \frac{1}{2\alpha\hat{x}(1+\tan^2\alpha)} - \frac{\hat{x}\tan\alpha}{(1-\tan^2\alpha)}. \tag{5.1}$$

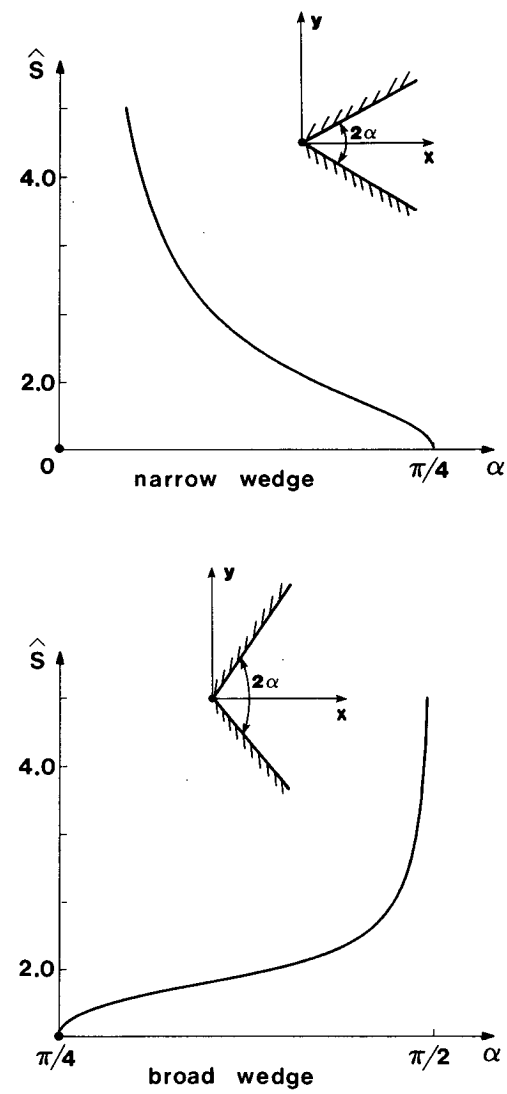

FIG. 6. The dependence of the distance between the separation point and the mouth ($\hat{S}$) on the wedge opening angle (α). Note that as α approaches $\pi/4$ from below (upper panel) and above (lower panel) the distance $\hat{S}$ goes to zero.

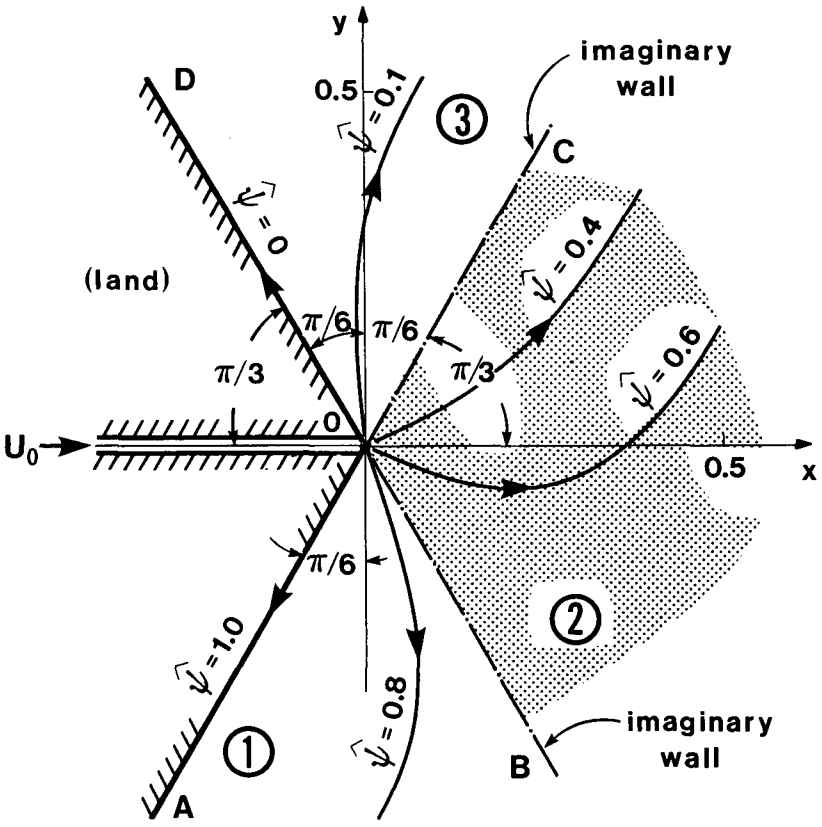

FIG. 7. The streamlines of an outflow spreading in a superbroad basin. The spreading can be thought of as consisting of three different regions because the extension of the coastlines act as effective walls. In regions 1 and 3 (i.e., unshaded sections confined by AOB and DOC) the flow deflects to the right (narrow basins) whereas in region 2 (i.e., shaded area confined by COB) the flow migrates toward the left (broad basin).

This relationship shows that when $\alpha < \pi/4$ (narrow basins) the velocity along the left wall decreases away from the source and vanishes at

$$\hat{x}_v = \left[\frac{1-\tan^2\alpha}{2\alpha\tan\alpha(1+\tan^2\alpha)}\right]^{1/2} \tag{5.2}$$

where the subscript v indicates that the variable in question is associated with vanishing speed. Note that along the wall the total velocity vanishes when $u^{(0)} = v^{(0)}/\tan\alpha$, and that elsewhere in the basin $u^{(0)} > 0$ for all $\hat{y}$ and $\hat{x}$ smaller than $\hat{x}_v$.

Along the wall the flow cannot advance farther than $\hat{x}_v$ because for $\hat{x} > \hat{x}_v$ the velocity becomes negative [according to (5.1)], corresponding to streamlines that do not originate upstream and are, therefore, impossible. It follows that at $\hat{x}_v$ the flow must separate from the left wall. In other words, for the radiation condition to be satisfied we must allow the flow to detach from the coast. Beyond the detachment the flow is bounded by a free streamline on the left and a wall on the right. A typical solution that includes the separation point for a narrow wedge is shown in Fig. 5a. We see that the separation is consistent with the general direction of deflection discussed earlier. Because of the tendency to deflect to the right, a parcel advancing along the left wall reaches a point where it can no longer cling to it.

For a narrow wedge, the solution (4.3) is valid as long as $\hat{x} \leqslant \hat{x}_v$, but it is not valid for $\hat{x} > \hat{x}_v$; in such regions the boundary conditions that we used for the walls (3.17ab) are no longer relevant and should be replaced by new conditions that involve the unknown location of the free separating streamline. The solution for the separated outflow (i.e., for $\hat{x} > \hat{x}_v$) is beyond the scope of this study. It is pointed out, however, that the new boundary conditions involve a new condition on the velocity along the separating streamline. The condition is that $\frac{1}{2}(u^2 + v^2)$ be constant along the free dividing streamline. It stems from the continuity of pressure and compensates for the fact that the location and shape of the free separating streamline are not given a priori (e.g., see Batchelor, 1967; Garabedian, 1964; Milne-Thomson, 1960).

A typical solution that includes the separation point for a broad wedge is shown in Fig. 5b. Note that for both the narrow and broad wedges the width of the

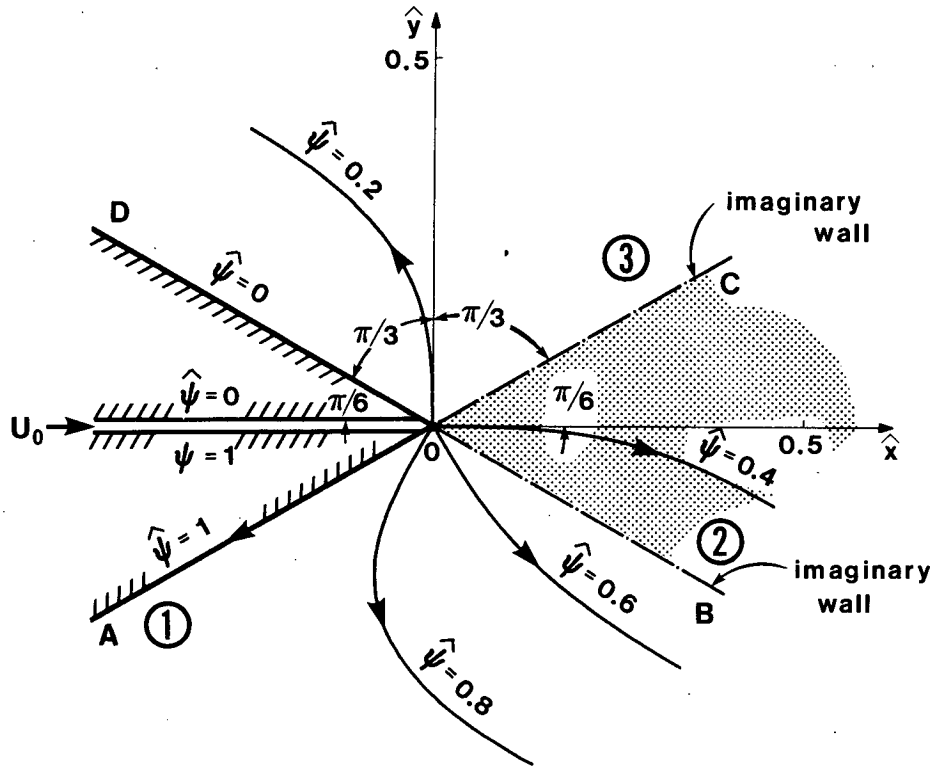

FIG. 8. The streamlines of an outflow spreading in an ultrabroad basin. As in Fig. 7, the outflow can be thought of as consisting of three separate basins. In basins 1 and 3 (i.e., unshaded sections confined by AOB and DOC) the flow deflects to the left (broad basins) whereas in basin 2 (i.e., shaded area confined by COB) the flow migrates toward the right (narrow basin).

separated outflow is of O(1), indicating that our new outflow length scale "l" is the appropriate scale for the problem. It illustrates that the outflow width cannot grow beyond this length scale. When the basin becomes wider than l, the outflow simply separates from the wall in order to maintain a width of O(l).

Before proceeding to super and ultra broad basins, it is appropriate to comment on the nature of the singularity occurring when $\alpha \to \pi/4$. The nature of the singularity can be understood by examining the first-order equations and the sensitivity of the distance between the detachment point and the source ($\hat{S} = \hat{x}_v/\cos\alpha$) to α. The structure of the first-order equations for both case I and case II [i.e., (3.12), (3.15)] shows that $\psi^{(1)} \sim O(\psi^{(0)})$ so that the perturbation scheme is valid as long as ϵ is small compared to unity. The sensitivity of $\hat{S}$ to α is shown in Fig. 6, which indicates that as α approaches $\pi/4$ from below (i.e., $\alpha < \pi/4$) or above (i.e., $\alpha > \pi/4$) the width of the separated outflow becomes small so that our new length scale l is no longer the proper length scale for the flow in the basin and ϵ is no longer small. Consequently, the first-order terms, $\epsilon\psi^{(1)}$, are of the same order as the zero-order terms and the perturbation scheme breaks down. This illustrates that the singularity is merely an indication that the detachment point is located very close to the source.

To obtain the proper solution for $\alpha \to \pi/4$ it is necessary to rescale the variables and take the length scale in the basin (l) to be equal to b. That is, ϵ must be taken to be unity and the full nonlinear equations should be solved. This is beyond the scope of this study.

b. Super and ultra broad basins

The dynamics of these extra broad basins is more complicated than those discussed in the previous subsection. In contrast to outflows spreading in basins with $\alpha < \pi/2$, which consist of a single current, outflows spreading in super and ultra broad basins bifurcate and form two currents (Figs. 7 and 8). The bifurcation results from the fact that the particular solution $\psi_p^{(0)}$ does not vanish only along the coastlines but also along their extensions into the ocean interior (see Figs. 7 and 8). Consequently, those extensions act as "imaginary walls" that divide the basin into three smaller sub-basins. In each of these sub-basins the outflow behaves as if it were spreading in it independently. Namely, it deflects to the right when the sub-basin is narrow ($\alpha < \pi/4$) and to the left when it is broad ($\alpha > \pi/4$). As a result, different directions of deflection occur in the basin and this forces the bifurcation.

At distance O(l) from the source there is a detach-

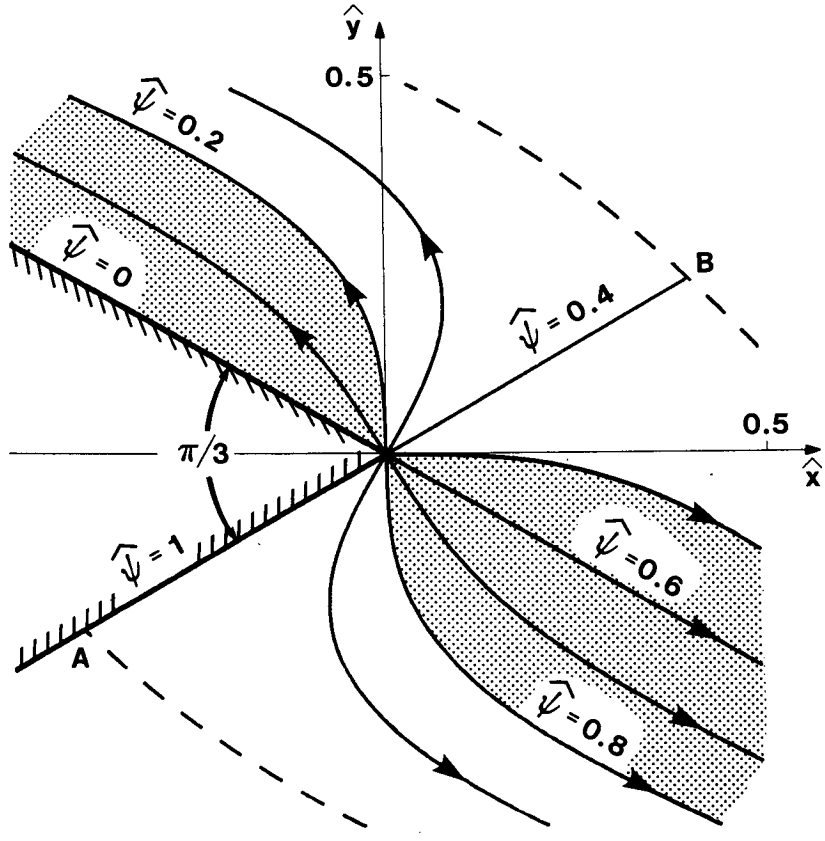

FIG. 9. The bifurcation of an outflow spreading in an ultrabroad basin. Note that for $\alpha = 5\pi/6$, 60% of the outflow flows to the right (as an isolated current) and 40% flows to the left. As before, the solution was extrapolated for a short distance beyond the separation and detachment points (dashed lines). Shaded areas correspond to the core of the currents.

ment from the walls, and portions of the basin's interior are blocked. The nature of this blocking is equivalent to that of a separation from the walls, except that it occurs in the interior of the basin because it is associated with the imaginary walls. Figure 9 shows that an outflow spreading in an ultra broad basin (i.e., $3\pi/4 \leqslant \alpha \leqslant \pi$) bifurcates into a narrow minor current that flows to the left and a broad major current that deflects to the right. By contrast, an outflow spreading in a super broad basin (i.e., $\pi/2 \leqslant \alpha \leqslant 3\pi/4$) bifurcates into a narrow minor current that deflects to the right and a major current that deflects to the left (Fig. 10).

The singularity at $\alpha = 3\pi/4$ represents, as previously, the condition at which the separation and blocking are located within a distance of $O(\epsilon)$ from the origin. When $\alpha \rightarrow 3\pi/4$ from above (i.e., $\alpha > 3\pi/4$) the separation from the left wall approaches the origin, whereas when α approaches $3\pi/4$ from below (i.e., $\alpha < 3\pi/4$) the separation from the right wall approaches the origin.

c. *The Tsugaru Strait*

Before considering the detailed application of the theory to the Tsugaru Strait, the reader should be warned that the application is largely conjectural. Namely, we shall point out that there are some encouraging similarities between the proposed model and the observed features, but we shall not reach any definite conclusions. This is mainly a result of the simplicity of the model and the limited observational data.

The Tsugaru Strait connects the Sea of Japan with the North Pacific (Fig. 11); it lies between the islands of Honshu and Hokkaido and is approximately 20 km wide at its eastern and western narrows. The average transport through the strait is roughly two Sverdrups (1 Sv $\equiv 10^6$ m^3 s^{-1}) (e.g., see Conlon 1981, 1982), and there is a large seasonal variability in the stratifications. During the cold season (January–June) the average density on the outflow side is roughly 1.0262 g cm^{-3}, whereas during the warm season (July–December) the density is much smaller, about 1.0247 g cm^{-3} (Conlon, 1981, 1982). The lower-layer density on the outflow side is about 1.0265; it remains approximately constant during the year.

In most parts of the strait—except perhaps the easternmost part (141°20′E) for which there is almost no data—the flow is in the same direction from top to

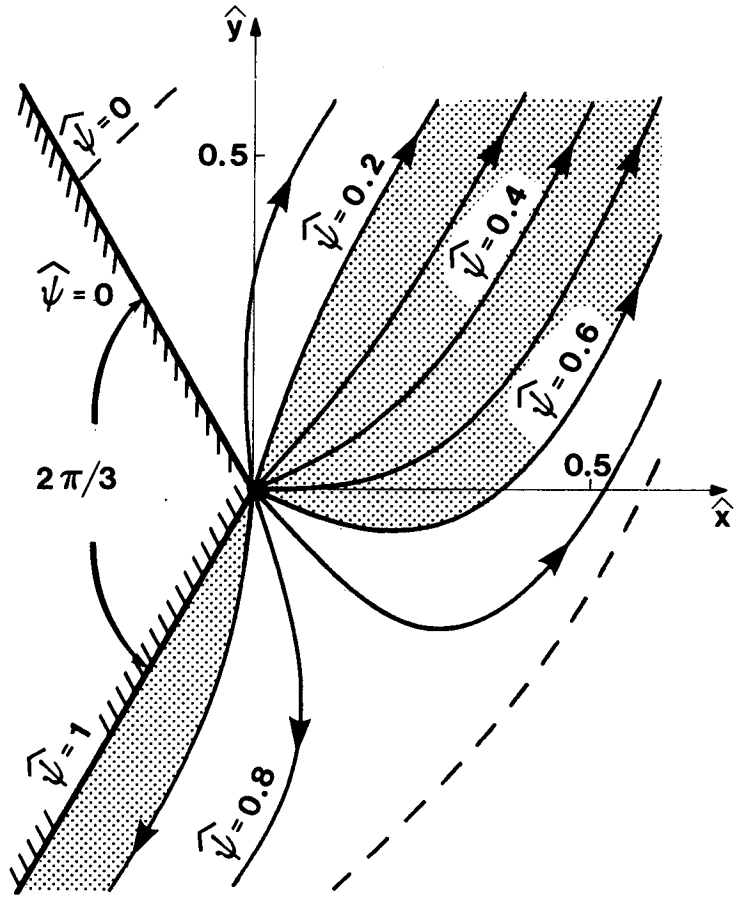

FIG. 10. As in Fig. 9 but for an outflow spreading in a superbroad basin. For $\alpha = 2\pi/3$, 75% of the outflow deflects to the left and penetrates into the interior as an isolated current. The remaining 25% deflects to the right and flows along the coast. Shaded areas correspond to the core of the currents.

bottom (Conlon, 1981, Sonu, 1981). For this reason, what we have termed the "case II model" is probably more relevant than case I. Recall, however, that to zero-order there is no difference between the two solutions.

Following Conlon (1981), the local topography, and the approximate geometry of the coastline shown in Fig. 11, we choose the following values as typical for the flow in the eastern narrows (Toi to Oma Saki) and the Tsugaru outflow:

$$\left.\begin{array}{l} \alpha \sim 120°,\ U_0 \sim 1.5\ \mathrm{m\ s^{-1}},\ 2b \sim 10\,\mathrm{km}, \\ \quad H \sim 150\,\mathrm{m},\ f \sim 10^{-4}\,\mathrm{s^{-1}} \\ g' \approx 2.7\times 10^{-2}\ \mathrm{m\ s^{-2}}\ \text{(warmer months)} \\ g' \approx 3.0\times 10^{-3}\ \mathrm{m\ s^{-2}}\ \text{(colder months)} \end{array}\right\} . \quad (5.3)$$

We chose the eastern narrows to be representative of the eastern strait width because observations suggest that the narrows control the width even in the area that is 30 km to the east. This is apparently achieved by side wall eddies which, in the area to the east of the narrows, prevent the strait core from being in a direct contact with the walls (see Fig. 14 in Conlon, 1981). A more accurate way of representing the actual strait is to include the narrow wedgelike widening immediately to the east of the narrows. However, such an inclusion would require a much more complicated model and is beyond the scope of this study. The strait average width ($\sim$10 km) was taken to be half the distance between the two coastlines at the surface of the eastern narrows because the strait cross section resembles a triangle. Note that the transport associated with (5.3) is $\sim$2.2 Sv, which is in agreement with the observed mass flux.

With the above values we have

$$\left.\begin{array}{l} \mathrm{Ro} \sim 3.0,\ \mathrm{Fr}_w \sim 0.5,\ \mathrm{Fr}_c \sim 5,\ \alpha \sim 120° \\ \quad \epsilon_w = 0.4,\ \epsilon_c = 1.73,\ l_w = 25\,\mathrm{km},\ l_c \sim 8\,\mathrm{km} \\ R_{dw} \sim 20\,\mathrm{km},\ R_{dc} \sim 7\,\mathrm{km} \end{array}\right\} \quad (5.4)$$

where the subscripts w and c indicate that the variable in question is associated with the warm or cold season, respectively. Note that the channel depth that we chose

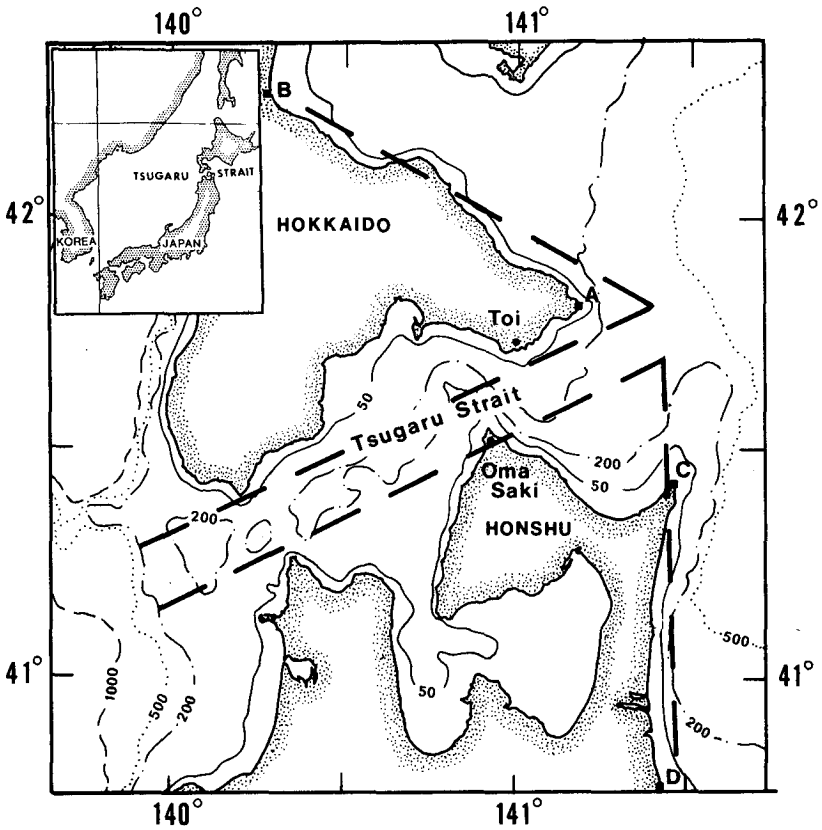

FIG. 11. The topography and shape of the Tsugaru Strait. Note that the coast can be approximated by straight lines (thick dashed lines) so that the flow from the Tsugaru Strait into the Pacific resembles the flow from a delta. A potentially serious drawback of this geometrical simplification is the fact that the widening in the area immediately to the east of Toi and Oma Saki is not included. To include this feature it is necessary to consider a much more detailed and complicated model and this is beyond the scope of this study.

(150 m) is somewhat smaller than the mean depth used by Conlon (1981) for the *outflow* depth in the Pacific. Since there is spreading and deepening, the outflow depth in the Pacific is expected to be larger than the channel depth. Specifically, the ratio between the two depths is $1 + \mathrm{Fr}/2$ [see Eq. (3.15)] so that in the warm season our outflow depth is ~ 190 m, which is fairly close to Conlon's value (210 m). In addition, note that Conlon defined the deformation radius on the basis of the outflow depth, whereas we have defined it on the basis of the channel depth so that our values are somewhat smaller.

The numerical values given by (5.4) suggest that during the *warm* season the outflow might behave in the manner suggested by Fig. 10. Namely, the warm Tsugaru outflow corresponds to an outflow spreading in a *superbroad basin* and should, therefore, penetrate into the interior as a major branch directed toward the northeast and a minor branch that should hug the coast and flow to the south. Several observations provide encouraging similarities. For instance, Fig. 12 displays the trajectories of drift bottles. Although such trajectories are difficult to interpret, they suggest that bifurcation is possible. According to these trajectories, the majority of the flow is directed toward the northeast, as suggested by Fig. 10. We shall see shortly that it is difficult to say whether the weak southward flow displayed by Fig. 10 is presented in the actual outflow, but this is not of major importance to our present discussion. Our main point is that *most of the flow* is indeed directed toward the northeast. The analysis of Conlon (1981, 1982) also supports the conjecture that the main part of the outflow penetrates into the Pacific Ocean as an isolated current (Fig. 13).

Conlon defined two outflow modes: the so-called gyre mode, where the warm outflow veers to the left and penetrates far into the Pacific, and a "coastal mode," which corresponds to a cold current flowing along the southern coast. As far as the *cold* season and the coastal mode are concerned, our model provides no information because, for this time of the year, the ratio between the channel width and the length scale in the open ocean is considerably larger than unity ($\epsilon_c = 1.73$) so that our perturbation scheme cannot be

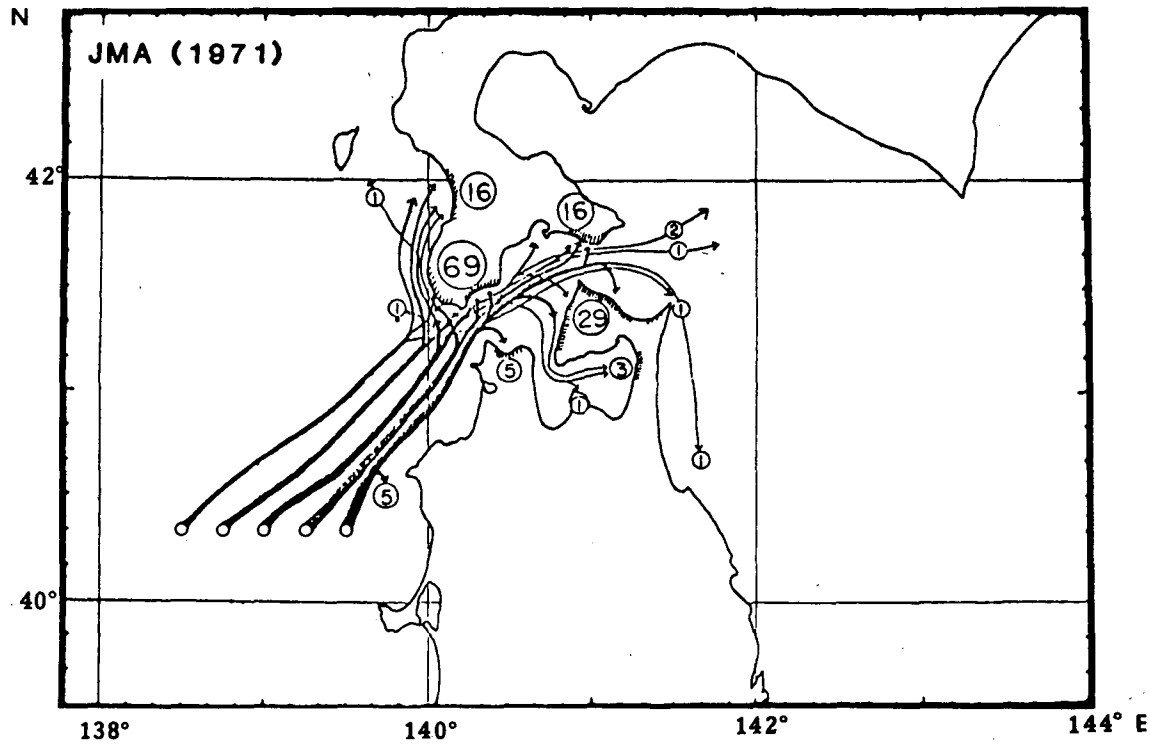

FIG. 12. Drift bottles trajectories in the Tsugaru Strait. Numbers indicate number of bottles collected in the various regions (adapted from Sonu, 1981). Note that five have drifted through the eastern narrows into the Pacific Ocean. Of these, two went to the right near the coast and three drifted into the interior in a similar fashion to the predicted bifurcation (Fig. 10).

applied. The warm season and the gyre mode, however, provide an encouraging similarity to Fig. 10 because it shows that the main part of the flow penetrates to the ocean as an isolated current.

Two aspects should be mentioned regarding Conlon's observations and their relationship to our model. First, it is important to realize that the only section of Fig. 13 relevant to our discussion is the vicinity of the mouth. Namely, the major part of the gyre and the downstream bifurcation resulting from the jet impinging on the coast (e.g., see Whitehead, 1985) are governed by phenomena in the basin and are not related to the processes in question. These parts of the flow are more than several length scales away from the mouth so that they do not represent a part of our model. Second, in the area to the south of the mouth there appears to be a contradiction between the flow pattern displayed by Fig. 12 and that displayed by Fig. 13. Conlon's analysis (Fig. 13) suggests a northward flow whereas the drift bottle trajectories (Fig. 12) suggest a southward flow. This apparent discrepancy is probably a result of the fact that very close to the coast the flow is directed southward, whereas away from the coast it is directed northward (Conlon, personal communication, 1985). Whatever the direction of the circulation in this area is, it is not of major importance to our application because most of the flow is directed toward the northeast.

Finally, it should be pointed out that the two-mode behavior is also in apparent agreement with the laboratory experiments of Whitehead and Miller (1979), who examined the behavior of a jet bounded by a front on the left-hand side. They established the criteria that for small deformation radii a mode similar to the "coastal mode" is established whereas for large deformation radii the flow forms a gyre. While it is certainly possible that the Tsugaru outflow is strongly dependent on the presence of a front, our present model suggests that a front may not be essential and that the warm gyre may be a part of a bifurcated outflow.

Before summarizing our results, it should be pointed out that while the above comparison and application are encouraging they do not provide a conclusive description of the flow pattern. Many refinements of the model are necessary before a definite conclusion can be reached. In particular, it is desirable to include the widening of the strait to the east of the narrows. Such a feature cannot be handled independently because it is not very long compared to l_w. We cannot consider this widening to be associated with an outflow spread-

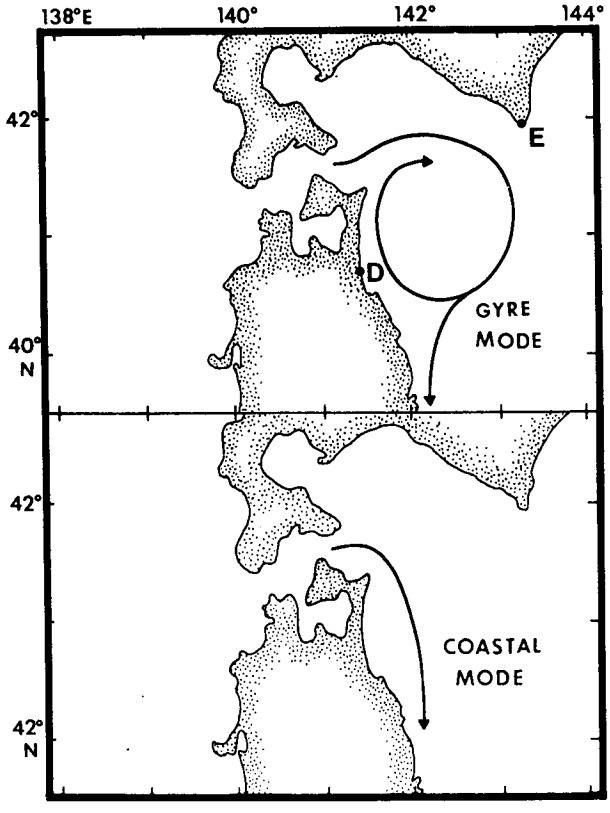

FIG. 13. Schematic diagram of the two outflow modes of the Tsugaru Strait. During the warm season (July–December) the outflow displays a gyre mode (upper panel) whereas during the cold season (January–June) it displays a coastal mode (lower panel). (Adapted from Conlon, 1982.) Note that the coastal mode cannot be examined with our model because the numerical values of its various parameters do not permit the use of our perturbation scheme. The upstream part of the outflow associated with the gyre mode is consistent with the main aspect of the predicted bifurcation (Fig. 10). Specifically, the section of the gyre in the immediate vicinity of the mouth [i.e., within several outflow length scales (l_w)] displays a penetration to the ocean interior that is similar to the *main branch* displayed in Fig. 10. Note that, (i) the apparent discrepancy between the presently displayed flow pattern and the one showed by Fig. 12 in the area to the south of the mouth is probably a result of the fact that these two weak flows are located in different areas (see text), and (ii) the scale of the gyre (~100 km) and the downstream bifurcation resulting from the jet impinging on the coastline are not related to the processes under discussion. These features are far from the mouth, and, therefore, they are governed by processes such as the width of the basin (i.e., the distance between E and D), which is not taken into account in our model.

ing in a narrow basin of the kind shown in Fig. 5a because such an application requires the basin to be much longer than the outflow length scale l_w to assure that there is no influence of the downstream area. In the region in question the length of the "basin" (Toi to point A) is about 20 km, which is roughly the same as l_w. An effective way of dealing with this issue would be to develop a numerical model that includes the delta as well as the widening between Toi and point A.

6. Summary

In this paper, an analytical model for the behavior of outflows on an f-plane is presented. The model has been developed under the assumptions that (i) the ocean can be approximated by a shallow upper layer and a very deep lower layer, which can be taken to be motionless; (ii) the motion is steady, frictionless and nondiffusive; and (iii) the effects of coastline irregularities and the influence of longshore coastal currents can be neglected. In reality, these processes will, no doubt, influence the flow. Although much work remains to be done before we can adequately understand the behavior of the real system, our present analysis gives useful information about the outflow.

The results of the theory can be summarized as follows.

(i) For an f-plane outflow there is a length scale (l) that differs from both the Rossby deformation radius and the channel width. It is given by $2R_d/(\mathrm{Ro})^{(1/2)}$, where R_d is the deformation radius $[(g'H)^{1/2}/f$ with g' the reduced gravity and H the feeding channel depth] and Ro is the Rossby number based on the upstream channel flow $[U_0/fb$ with U_0 the speed in the channel and b half the channel width]. For some wide straits, Ro ~ O(1) so that $l \sim O(R_d)$, but for many channels, particularly those in low latitudes, Ro $\gg$ 1 so that $l \ll R_d$.

(ii) The above length scale is the *maximum* width that the outflow can attain. In regions where the basin width is larger than l, the outflow separates from one of the walls, and, by doing so, it maintains its own width (l).

(iii) The length scale (l) is a consequence of the fact that as an outflow spreads in the ocean, the fluid gains cyclonic vorticity to compensate for the increase in depth, which results from the decrease in speed. An additional result of this latter process is that the fluid does not spread uniformly in all directions (as nonrotating outflow would do) but rather is deflected toward one of the side walls. When the angle between the two walls is smaller than $\pi/2$, the cyclonic vorticity generated by the spreading is offset mainly by generation of horizontal shear. In contrast, when the angle is wider than $\pi/2$ the cyclonic vorticity is compensated mainly by curvature vorticity. In the latter case the outflow migrates toward the left wall (in the Northern Hemisphere), whereas in the former the outflow deflects to the right.

(iv) When the basin into which the outflow debouches is very broad (i.e., the continent resembles a delta) the outflow bifurcates. It splits into two branches—a minor current that flows along one of the walls and a major current that is penetrating into the ocean interior as an isolated current. The bifurcation results from the fact that the extensions of the coastlines

into the ocean interior act as dividing "walls." These imaginary walls create three sub-basins, each of which behaves as if an independent outflow is spreading in it. Consequently, the parent basin contains few different deflections and this causes the formation of two independent currents.

The last prediction (iv) was compared to the observed structure in the Tsugaru strait, and encouraging, but inconclusive, agreement was generally noted.

Acknowledgments. This study was supported by the Office of Naval Research Grant N00014-82-C-0404. Conversations with D. Conlon regarding the observational part of the problem were very useful. S. Murray and two anonymous reviewers provided helpful comments on an earlier version of this paper. Computer-generated plots were made by S. Van Gorder.

REFERENCES

Batchelor, G. K., 1967: *An Introduction to Fluid Dynamics.* Cambridge University Press, 615 pp.

Beardsley, R. C., and J. Hart, 1978: A simple model for the flow of an estuary onto a continental shelf. *J. Geophys. Res.,* **53,** 873–883.

Conlon, D. M., 1981: Dynamics of flow in the region of the Tsugaru Strait. Coastal Studies Inst. Tech. Rep. No. 312, Louisiana State University, 61 pp.

——, 1982: On the outflow modes of the Tsugaru warm current. *La mer,* **20,** 60–64.

Garabedian, P. R., 1964: *Partial Differential Equations.* Wiley and Sons, 672 pp.

Gill, A. E., 1982: *Atmosphere Ocean Dynamics.* Academic Press, 662 pp.

Griffith, R. W., and E. J. Hopfinger, 1983: Gravity currents moving along a lateral boundary in a rotating fluid. *J. Fluid Mech.,* **134,** 357–399.

Ingersoll, A. P., 1969: Inertial Taylor columns and Jupiter's Great Red Spot. *J. Atmos. Sci.,* **26,** 744–752.

Kawasaki, Y., and T. Sugimoto (with Editor's note), 1984: Experimental studies on the formation and degeneration processes of the Tsugaru warm gyre. *Ocean Hydrodynamics of the Japan and East China Sea,* T. Ichye, Ed., 423 pp.

Milne-Thomson, L. M., 1960: *Theoretical Hydrodynamics.* Macmillan, 660 pp.

Nof, D., 1978a: On geostrophic adjustment in sea straits and wide estuaries: Theory and laboratory experiments. Part I: One-layer system. *J. Phys. Oceanogr.,* **8,** 690–702.

——, 1978b: On geostrophic adjustment in sea straits and wide estuaries: Theory and laboratory experiments. Part II: Two-layer system. *J. Phys. Oceanogr.,* **8,** 861–872.

——, 1981: On the dynamics of equatorial outflows with application to the Amazon's basin. *J. Mar. Res.,* **39,** 1–29.

Paul, J., and W. Lick, 1974: A numerical model for thermal plumes and rivers discharge. *Proc. 17th Conf. on Great Lakes Research,* Ann Arbor, Int. Assoc. Great Lakes Res., 445–455.

Sonu, C. J., 1981: Survey of sea strait data around Japan. Tech. Rep. No. 1, Tekmarine, Inc., Sierra Madre, 297 pp.

Stern, M. E., 1980: Geostrophic fronts, bores, breaking and blocking waves. *J. Fluid Mech.,* **99,** 687–703.

——, J. A. Whitehead and B. L. Hua, 1982: The intrusion of a density current along the coast of a rotating fluid. *J. Fluid Mech.,* **123,** 237–265.

Stommel, H., A. B. Arons and A. J. Faller, 1958: Some examples of stationary planetary flow patterns in bounded basins. *Tellus,* **10,** 179–187.

Takano, K., 1954: On the velocity distribution off the mouth of a river. *J. Oceanogr. Soc. Japan,* **10,** 60–64.

——, 1955: A complementary note on the diffusion of the seaward river flow off the mouth. *J. Oceanogr. Soc. Japan,* **11,** 147–149.

Whitehead, J. A., 1985: The deflection of a baroclinic jet by a wall in a rotating fluid. *J. Fluid Mech.,* **157,** 79–93.

——, and A. R. Miller, 1979: Laboratory simulation of the gyre in the Alboran Sea. *J. Geophys. Res.,* **84,** 3733–3742.

——, A. Leetmaa and R. A. Knox, 1974: Rotating hydraulics of strait and sill flows. *Geophys. Fluid Dyn.,* **6,** 101–125.